Progress In Electromagnetics Research B, Vol. 37, 387–401, 2012

EXPERIMENTAL OBSERVATION OF LINEAR AND NONLINEAR PULSES IN TRAVELING-WAVE FIELD-EFFECT TRANSISTORS PERIODICALLY LOADED WITH SCHOTTKY VARACTORS

R. Sugai, T. Shima, and K. Narahara*

Graduate School of Science and Engineering, Yamagata University, 4-3-16 Jonan, Yonezawa, Yamagata 992-8510, Japan

Abstract—We characterize the pulse propagation on a traveling-wave field-effect transistor (TWFET) with the drain line periodically loaded with Schottky varactors for short pulse amplification. Owing to the coupling between the gate and drain lines, two propagation modes are developed on a TWFET. It is expected that the pulses carried by one of the two modes are uniquely amplified, whereas those carried by the other mode are attenuated. By properly introducing nonlinearity via the loaded varactors, the proposed TWFET succeeds in the amplification of short pulses by compensating for dispersive distortions. This study verifies the design criteria for the amplification of short pulses in TWFETs through the experimental observation of the properties of the linear and nonlinear pulses on a TWFET.

1. INTRODUCTION

Schottky varactors have been extensively used in nonlinear transmission lines (NLTLs). Originally, NLTLs were used for the development of Toda solitons [1]. Carefully designed Schottky varactors are employed in electronic circuits including electrical shock [2] and harmonic wave generators [3, 4]. Recently, Kintis et al. [5] proposed a NLTL pulse generator using two NLTLs. Yildirim et al. [6] proposed a method for generating a periodic, short pulse train using a NLTL connected with an amplifier. Moreover, a coupled NLTL with strong dispersion has been investigated based on the nonlinear Schrödinger equation [7]. Weakly dispersive coupled NLTLs are characterized to develop high repetition-rate pulse trains [8, 9].

Received 6 November 2011, Accepted 31 December 2011, Scheduled 8 January 2012

* Corresponding author: Koichi Narahara (narahara@yz.yamagata-u.ac.jp).

Although various applications have been investigated for NLTLs, the line resistance generally attenuates the pulse amplitude, making pulses very small for a NLTL to exhibit nonlinearity. To extend the potential of nonlinear waves, a scheme is required to compensate for the losses or to amplify them. We consider a traveling-wave field-effect transistor (TWFET) [10] to realize such a scheme. A TWFET is a distributed device formulated by two transmission lines that are mutually coupled with the gate-drain capacitance, mutual inductance, and transconductance. By periodically introducing the Schottky varactors in the drain line, we consider TWFETs as the platform for the development of nonlinear solitary waves.

Owing to the coupling between the gate and drain lines, two different propagation modes called the c- and π-modes develop on a TWFET. Each mode has its own velocity, characteristic impedance, and voltage fraction between the gate and drain lines. It is expected that only pulses carried by one of the modes are amplified, whereas those carried by the other mode are attenuated [11]. In addition, it was found that the nonlinearity introduced by the gate-source and drain-source Schottky capacitors succeeds in compensating for the dispersive distortions of pulses carried by either mode because of properly designed signal inputs. As a result, TWFETs enable the amplification of large pulses that are not affected by either dispersion or attenuation.

First, we describe the fundamental properties of TWFETs, including the structure, the amplification of small linear pulses, and the Korteweg-de Vries (KdV) equation that governs the large pulses in TWFETs. Then, we discuss a method of amplifying the nonlinear pulses in a TWFET. Finally, we discuss experimental results that validate the design criteria and the supporting evidences obtained by numerical calculations.

2. NONLINEAR TWFETS

Figure 1 shows the schematic of the TWFET that we investigated. Figure 1(a) shows the bird's eye view of the device. Four electrode lines are set up on a surface where some dielectric passivation alternates the active region. Small FETs are formed periodically on the active regions. The lines labeled by S, G, and D correspond to the source, gate, and drain lines, respectively. A cross section corresponding to the active region is shown in Figure 1(b). Originally, the drain line is ohmic contacted on the active regions [12, 13]. In our case, it is formed, such that a part is ohmic contacted for flowing the FET drain-to-source current, and the remaining part is Schottky contacted. The

depletion region beneath the drain is designed to develop toward the adjacent electrode labeled by G_2. The equivalent circuit corresponding to the four lines on a single period of alternating active and passive regions is shown in Figure 1(c). Red and blue elements demonstrate the gate and drain lines, respectively. For an active region, the FET contribution is represented by the gate-source capacitance C_{gs}, gate-drain capacitance C_{gd}, and drain-source current I_{ds}. We neglected the influence of the gate current leakage. In addition, the varactor contribution is represented by a bias-dependent capacitance C_{ds}. On the other hand, a passive region is represented by the resistance R_g (R_d) and inductance L_g (L_d) for the gate (drain) line. When the gate line is in close proximity to the drain line, the mutual inductance between the lines L_m cannot be neglected. In general, the gate-source capacitance, C_{gs}, has a bias-dependence because of the Schottky contact beneath the gate. As a result, the gate and drain lines are modeled by NLTLs. These two are coupled via C_{gd}, L_m, and I_{ds}. We model the Schottky varactors to obtain the capacitance-voltage

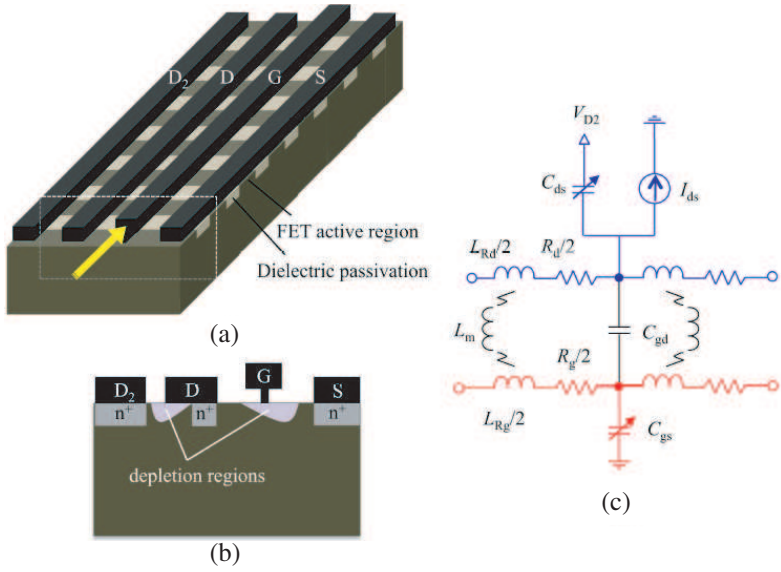

Figure 1. Schematic of the TWFET. (a) The bird's eye view, (b) cross section of a monolithically integrated TWFET, and (c) the equivalent circuit representing the unit-cell TWFET. Red and blue elements in Figure 1(c) illustrate the gate and drain lines, respectively. The drain line is periodically loaded with Schottky varactors.

relationship given by

$$C(V) = \frac{C_0}{\left(1 - \dfrac{V}{V_J}\right)^M}, \tag{1}$$

where V is the voltage across the terminals. C_0, V_J, and M are the optimizing parameters, which we denote as $C_1\,(C_2)$, $V_{J1}\,(V_{J2})$, and $M_1\,(M_2)$ for $C_{gs}\,(C_{ds})$, respectively. Note that $V < 0$ for the reverse bias case.

There are two different propagation modes, c- and π-modes, on a linear coupled line [14], and the same is true for a sub-threshold TWFET. Each mode has its own velocity and voltage fraction between the lines (= drain voltage/gate voltage). Hereafter, we denote the velocity of the c-mode, velocity of the π-mode, voltage fraction of the c-mode, and voltage fraction of the π-mode at long wavelengths as u_c, u_π, R_c, and R_π, respectively. These are explicitly written as

$$u_{c,\pi} = \sqrt{\frac{x_1 + x_2 \pm \sqrt{(x_1 + x_2)^2 - 4x_3}}{2x_3}}, \tag{2}$$

$$R_{c,\pi} = \frac{x_1 - x_2 \pm \sqrt{(x_1 + x_2)^2 - 4x_3}}{2C_{gd}L_g}, \tag{3}$$

where the upper (lower) signs are for the c (π)-mode. For concise notations, we define $x_{1,2,3}$ as

$$x_1 = C_{gs}(V_G)L_g + C_{gd}L_g, \tag{4}$$

$$x_2 = C_{ds}(-V_b)L_d + C_{gd}L_d, \tag{5}$$

$$x_3 = \left[C_{gs}(V_G)C_{ds}(-V_b) + C_{gs}(V_G)C_{gd} + C_{ds}(-V_b)C_{gd}\right] L_gL_d, \tag{6}$$

for the case where the gate and drain lines are biased at V_G and V_D, respectively, and we set $V_b = |V_D - V_{D2}|$.

Conveniently, the FET gain positively contributes to the π-mode, whereas the c-mode is attenuated to a greater degree. Therefore, the TWFET can be free from the wave distortions caused by the coexistence of the c- and π-modes. We denote the transconductance as G_m, then the per-unit-cell gains of the c- and π-modes, ν_c and ν_π, are given by

$$\begin{aligned}\nu_{c,\pi} = {} & \mp\frac{G_mC_{gd}L_gL_du_{c,\pi}^2}{2\sqrt{(x_1 + x_2)^2 - 4x_3}} - \frac{R_d}{4L_d} - \frac{R_g}{4L_g} \\ & - \left(\frac{R_d}{4L_d} - \frac{R_g}{4L_g}\right)\frac{x_1 - x_2}{\sqrt{(x_1 + x_2)^2 - 4x_3}},\end{aligned} \tag{7}$$

where the upper (lower) signs are for the c (π)-mode. By definition, the corresponding mode is amplified if $\nu > 0$. As a result, the π-mode is always the unique mode to be amplified if the first term on the right hand side of Eq. (7) surpasses the other terms. As long as a pulse travels on a unique mode, it is free from distortions caused by the dispersive difference between modes. By the π-mode excitation and the terminations with the π-mode impedances, we can suppress the wave distortions caused by either modal dispersion or multiple reflections. However, the π-mode also has weak but finite dispersion that becomes significant near the cutoff frequency. The short-wavelength waves travel more slowly than the long-wavelength waves due to dispersion, and results in the distortion of the baseband pulses that have short temporal durations. If we succeed in compensating this dispersive distortion of the π-mode, a TWFET can achieve short pulse amplification. We expect the dispersion-compensation using Schottky varactors. To quantify the compensation of dispersion by the nonlinearity, we apply the reductive perturbation to the transmission equations of a TWFET. As a result, both the c- and π-modes are known to support the KdV solitons [11]. The c- and π-mode solitons have voltage fractions of R_c and R_π, respectively. Moreover, the pulse width of the single KdV soliton carried by c (π)-modes, $P_{w,c(\pi)}$, is given by

$$P_{w,c(\pi)} = \frac{\sqrt{12p_{c(\pi)}/q_{c(\pi)}A_0}}{u_{c(\pi)} + q_{c(\pi)}A_0/3}, \tag{8}$$

where A_0 represents the pulse amplitude, and the dispersion and nonlinear coefficients, $p_{c(\pi)}$ and $q_{c(\pi)}$, are respectively given as

$$p_{c(\pi)} = \frac{u_{c(\pi)}}{24}, \tag{9}$$

$$q_{c(\pi)} = \mp\left(\frac{C_{gs}(V_G)C_{gd}L_g^2M_1}{2(V_G - V_{J1})} + \frac{C_{ds}(-V_b)C_{gd}L_d^2M_2}{2(-V_b - V_{J2})}\right) \times \frac{u_{c(\pi)}^3\left(x_1 - x_2 \mp \sqrt{(x_1+x_2)^2 - 4x_3}\right)}{\sqrt{(x_1+x_2)^2 - 4x_3}\left(x_1 - x_2 \pm \sqrt{(x_1+x_2)^2 - 4x_3}\right)}, \tag{10}$$

where the upper (lower) signs are for the c (π)-mode. Note that A_0 is set as positive (negative) for $p_{c(\pi)}q_{c(\pi)} > (<)0$. Figure 2(a) shows the π-mode voltage fraction for different values of V_b. To see the properties of our breadboard test line, we used the line parameters corresponding to the circuit elements of the test line, which are listed in Table 1. Note that M_1 is set to zero and we assume that there is no bias-dependence of C_{gs} and L_m is neglected. In addition, V_G and V_D are

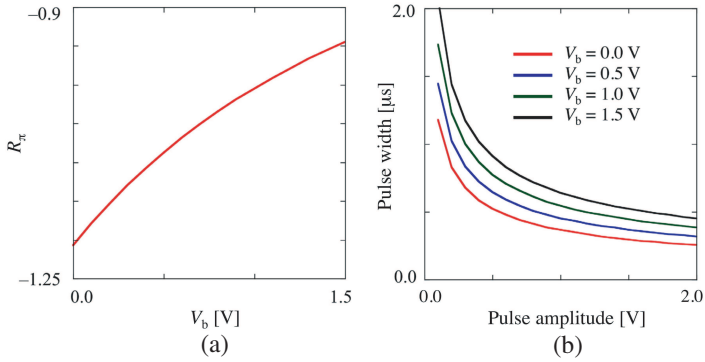

Figure 2. Dependence of line properties on voltage biasing Schottky varactor. (a) The voltage fraction between the gate and drain lines (drain amplitude/gate amplitude) and (b) the pulse widths of single solitons developed on a TWFET.

Table 1. Line parameters used to simulate measured results.

C_2 (pF)	65.0	C_1 (pF)	47.0
M_2	1.26	M_1	0.0
V_{J2} (V)	3.6	V_{J1} (V)	1.0
L_g (μH)	100.0	L_d (μH)	100.0
C_{gd} (pF)	47.0	L_m (μH)	0.0

set to −2.0 and 3.0 V, respectively. Referring to Eq. (1), the bias dependence of C_{ds} is weakened for large $|V_b|$. Moreover, R_π decreases in magnitude. Therefore, the nonlinearity of C_{ds} has a smaller effect on the π-mode pulse as $|V_b|$ increases. As a result, it becomes difficult to compensate for dispersions at large $|V_b|$. Figure 2(b) shows the dependence of the pulse width of a single KdV soliton on V_b, calculated by Eq. (8). Shorter pulses are influenced more by the dispersive distortions. Therefore, a stronger nonlinearity is required to compensate for the dispersion. In other words, we have to set $|V_b|$ sufficiently small to manage short pulses.

Figure 3 shows how to apply pulses to a TWFET. To develop the π-mode pulses, the input pulses applied to the gate and drain lines have dissimilar parities. In Figure 3(a), V_G is set below V_{th} and the gate pulse is applied in such a way that the pulse peak is above V_{th}. For dispersion compensation, we minimize the bias-dependence of C_{gs}. Moreover, the anode of C_{ds} has to be connected to the drain in each cell. In contrast, Figure 3(b) shows that V_G is set above V_{th} and the

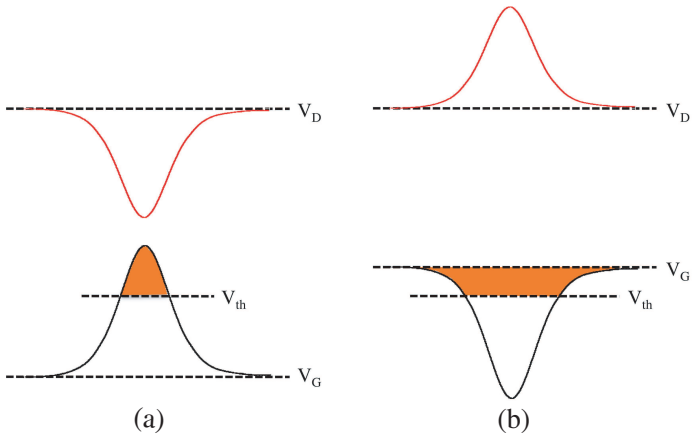

Figure 3. Methods of signal application. The gate and drain pulses have opposite parities. The gate pulse is input across V_{th}, such that (a) $V_G < V_{th}$ and (b) $V_G > V_{th}$. This study considers the case shown in (a).

gate pulse is applied in such a way that the pulse peak is below V_{th}. For dispersion compensation, the cathode of C_{ds} has to be connected to the drain in each cell. The former method is preferred, because it requires no steady-state drain current. The latter method should be used only when the nonlinearity of C_{gs} significantly surpasses that of C_{ds}.

3. EXPERIMENT

To examine the properties of nonlinear pulses in a practical situation, we carried out time-domain measurements of a TWFET. The equivalent circuit shown in Figure 1(c) was realized by using discrete circuit components assembled on a standard breadboard. The total cell number was 170. The top view of the test line is shown in Figure 4(a). The unit cell is enclosed by red dashed lines, which includes the type TDK EL0405 inductors L_g, L_d; TDK FK24C0G1 capacitors C_{gd}, C_{gs}; Toshiba 1SV101 varactor; and Toshiba 2SK30A JFET. The typical threshold voltage V_{th} of 2SK30A JFET is -1.5 V. Throughout the measurements, V_D was fixed at 3.0 V. The series inductance was 100 µH. Both the gate and mutual capacitances were 47 pF. These design parameters of the test line are summarized in Table 2. Figure 4(b) shows the schematic of the measurement setup. The gate and drain lines were fed by the signals generated by a NF-

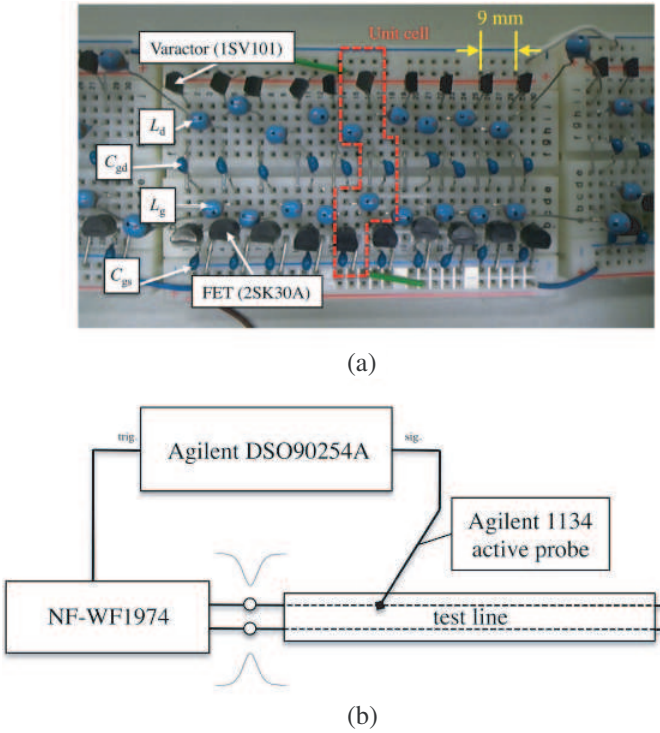

Figure 4. Experimental setup. (a) The top view of the test line and (b) measurement setup.

WF1974 two-channel function generator. The other end was used to feed bias voltage. The waveforms were detected by an Agilent 1134 active probe and monitored in the time domain using an Agilent DSO90254A oscilloscope. The probe impedance was sufficiently high to monitor the voltage at each cell without disturbing the signals on the line.

Figure 5 shows the small-signal response of the test line. We applied a 100-mV pulse to the gate line. The pulse splits into the c- and π-mode components. We can therefore simultaneously examine the property of the c- and π-mode pulses. V_b was set to $-2.0\,\mathrm{V}$, and four temporal waveforms were monitored at the points with 40-cell increments. Black and red curves show the waveforms on the gate and drain lines, respectively. Figure 5(a) shows the waveforms at $V_G = -2.0\,\mathrm{V}$ ($< V_{th}$). Moreover, black and red arrows indicate the π- and c-mode components, respectively. The c-mode pulses on the gate and drain lines have common parities and the π-mode pulses have

Table 2. Properties of test line.

FET threshold voltage (V)	−1.5
Drain bias voltage (V)	3.0
Total cell number	170
Gate capacitance (pF)	47.0
Mutual capacitance (pF)	47.0
Gate and Drain inductance (μH)	100.0

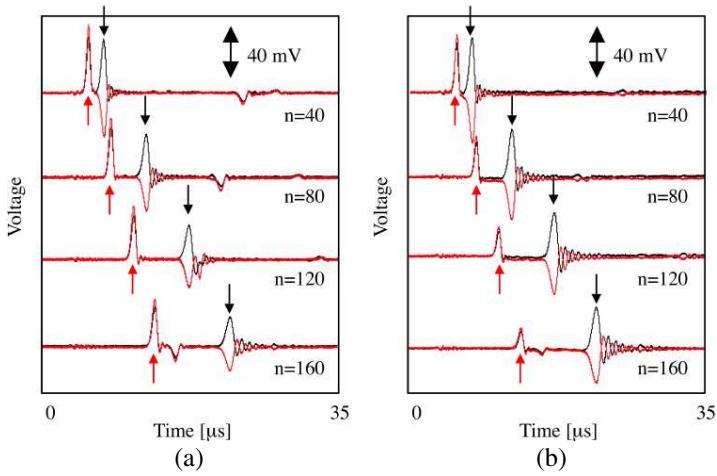

Figure 5. Measured small-signal response of a TWFET. Temporal waveforms monitored at $n = 30, 70, 110, 150$ are plotted for (a) $V_G = -2.0\,\mathrm{V}$ and (b) $V_G = -1.41\,\mathrm{V}$. Black and red curves show the waveforms on the gate and drain lines, respectively.

opposite parities. The peak amplitude decreases in both the c- and π-mode pulses because of the attenuation by the parasitic resistance of inductors and the dispersive distortions. Figure 5(b) represents the waveforms at $V_G = -1.41\,\mathrm{V}$ ($> V_{th}$). We can clearly see that both the incident and reflected c-mode pulses are more attenuated than those in Figure 5(a). In contrast, the π-mode pulses are less attenuated than those in Figure 5(a). As expected, the π-mode is the unique mode to be amplified, although the dispersive distortions of the π-mode pulses are significant, so that the pulse width is not preserved. Figure 6(a) shows the dependence of the c- and π-mode velocities on V_b. To estimate the velocities, we measured the temporal

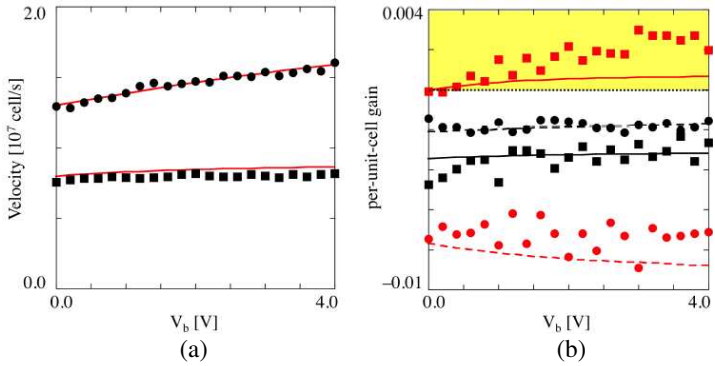

Figure 6. Properties of c- and π-mode pulses. (a) The velocities and (b) the per-unit-cell gain of the c- and π-mode pulses. In the hatched region in Figure 6(b), a pulse is amplified.

waveforms at two different cells and evaluated the delay for each pulse. The c- and π-mode quantities are shown by circles and squares in Figures 6(a) and (b), respectively. The red curves in Figure 6(a) are obtained by Eq. (2) with optimized values of C_2 (76 pF), M_2 (1.04), and V_{J2} (3.3 V). The Schottky varactors affect the wave propagation as expected. Figure 6(b) shows the dependence of the per-unit-cell gain for the c- and π-mode pulses on V_b. The black and red symbols show the per-unit-cell gains for $V_G = -2.0\,\mathrm{V}$ and $V_G = -1.41\,\mathrm{V}$, respectively. By definition, the pulse amplitude increases when the per-unit-cell becomes positive. At $V_G = -2.0\,\mathrm{V}$, the π-mode pulse is more attenuated than the c-mode pulse, whereas the π-mode pulse is uniquely amplified at $V_G = -1.41\,\mathrm{V}$. The solid and dashed curves in Figure 6(b) are obtained by estimating $\nu_{c,\pi}$ in Eq. (7). We set $R_{g,d}$ and G_m to $5.5\,\Omega$ and $1.8 \times 10^{-2}\,\mathrm{mS}$, respectively, which simulates the measured gain sufficiently.

We then measured the large-signal response of the test TWFET. To evaluate the properties of the π-mode, the input voltage fraction between the gate and drain channels of the input signal was set to $-1.0\,(\sim R_\pi)$ and the pulses were applied as shown in Figure 3(a). We set V_G and V_b to $-2.0\,\mathrm{V}$ and $0.0\,\mathrm{V}$, respectively. Figure 7(a) shows the temporal waveforms observed for $A_0 = 0.53\,\mathrm{V}$, such that the pulse peak was slightly above V_{th}. Although the pulse amplitude decreased gradually, the dispersive distortions were suppressed significantly, so that the pulse shape was almost preserved. As expected, the π-mode can support a dispersion-free nonlinear pulse. To observe the effect of the FET gain, A_0 was set to $0.60\,\mathrm{V}$; the measured waveforms are shown

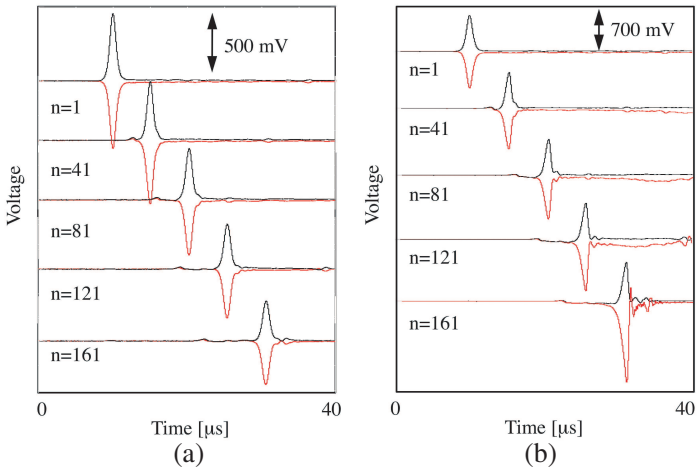

Figure 7. Measured large-signal response of a TWFET. Temporal waveforms monitored at $n = 1$, 41, 81, 121, and 161 are plotted for the input amplitudes of (a) 0.53 V and (b) 0.60 V. Black and red curves show the waveforms on the gate and drain lines, respectively.

in Figure 7(b). It was found that the π-mode was uniquely amplified even for a nonlinear pulse. Because the FET gain affects the pulse at only partial voltage levels, the waveform was altered, such that the fall-time was significantly decreased and the rise-time was almost preserved at $n = 161$. The amplitude was almost unchanged up to $n = 81$ and then increased rapidly. The growth rate was larger in the drain line than in the gate line, and the voltage fraction of the π-mode was therefore larger in magnitude than that of the original π-mode. This discrepancy in the voltage fraction resulted in the development of the c-mode waves preceding the original π-mode pulse. For larger growth rates, the extent of the new c-mode waves increased to significantly influence the original π-mode pulse. V_G, V_b, and A_0 have to be designed to minimize the new c-mode waves. In general, the nonlinear pulse in a TWFET is free from both the mode and line dispersions. Therefore, the TWFET is able to amplify the pulses without deteriorating their steepness.

Figure 8 shows the spatial variation of the peak amplitude of the π-mode pulse along the gate line for different values of A_0. The amplitude decreased monotonically for an input amplitude of ≤ 0.58 V ($\equiv A_{th}$). In contrast, the pulse was amplified significantly for amplitudes larger than A_{th}. Because the growth rate was exponential, it depends to a larger extent on the input amplitude.

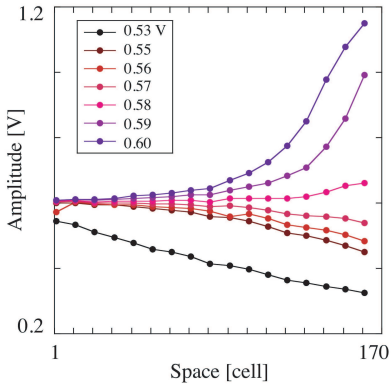

Figure 8. The spatial variation of the peak-amplitude on the gate line.

4. DISCUSSION

It was experimentally verified that the π-mode pulse is uniquely amplified irrespective of the pulse amplitude, such that the TWFET effectively preserves the pulse steepness. In this section, we examine the advantage obtained by introducing Schottky varactors through numerical calculations that simulate the measurements. The line voltages of the gate and drain lines at the nth cell are denoted as V_n and W_n, respectively, and the line currents of the gate and drain lines flowing in the nth cell are denoted as I_n and J_n, respectively. The transmission equations of a TWFET are then given by

$$V_{n-1} - V_n = L_g \frac{dI_n}{dt} + R_g I_n, \tag{11}$$

$$W_{n-1} - W_n = L_d \frac{dJ_n}{dt} + R_d J_n, \tag{12}$$

$$I_n - I_{n+1} = [C_{gd} + C_{gs}(V_n)] \frac{dV_n}{dt} - C_{gd} \frac{dW_n}{dt}, \tag{13}$$

$$J_n - J_{n+1} = [C_{gd} + C_{ds}(W_n - V_{D2})] \frac{dW_n}{dt} - C_{gd} \frac{dV_n}{dt} + I_{ds}(V_n, W_n), \tag{14}$$

where $I_{ds}(V) = \beta(V - V_{th})^2$ with β and V_{th} being $0.9\,\mathrm{mA/V^2}$ and $-1.5\,\mathrm{V}$, respectively. We numerically solved Eqs. (11) to (14) using the fourth-order Runge-Kutta method. For $C_{gs,gd}$ and $L_{g,d}$, we used the values listed in Table 1. R_g and R_d were set to $5.5\,\Omega$. Moreover, we employed Eq. (1) for C_{ds} setting C_2, M_2, and V_{J2} to 76 pF, 1.04, and 3.3 V, respectively.

The effect of the nonlinearity is shown in Figure 9, which shows the calculated large-signal response of a TWFET. Figures 9(a) and (b) show the five temporal waveforms monitored for a common input pulse at $n = 5, 45, 85, 125$, and 165 for the linear and nonlinear TWFETs, respectively. For the linear TWFET, we fixed the value of C_{ds} to $C(V_D - V_{D2})$. The FET was found to have no contribution to the traveling pulses when the pulse peak becomes less than V_{th}. Originally, the nonlinearity recovers the dispersive decrease in amplitude. Therefore, the nonlinear TWFET can amplify the relatively small pulses that cannot be amplified in a linear TWFET. As expected, we observed in Figure 9 that the pulse cannot maintain its amplitude in the linear TWFET, whereas the nonlinear TWFET succeeds in amplification.

Finally, we examined the properties of amplified pulses. The total cell number was set to 500 and the input amplitude was tuned to establish unity gain. Figures 10(a) and (b) show the calculated waveforms monitored at $n = 100$, 200, 300, and 400 for the nonlinear and linear TWFETs, respectively. In Figure 10(a), the π-mode pulse travels steadily and the pulse shape is almost unaltered at $n = 400$. On the other hand, the pulse is gradually distorted by dispersion

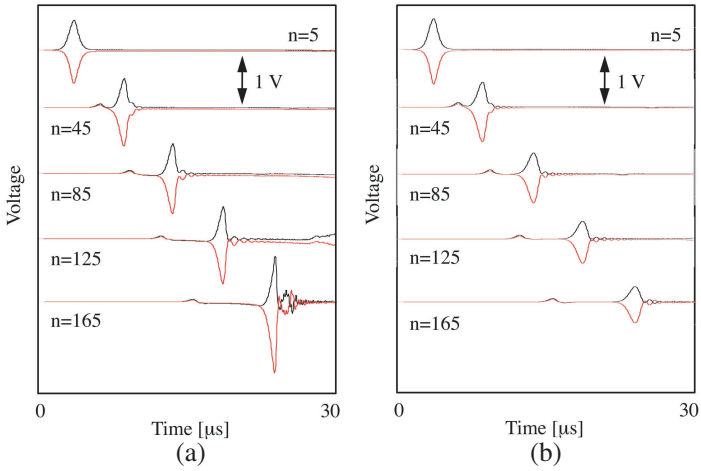

Figure 9. Calculated large-signal response of a TWFET. The total cell number was set to 170. Five temporal waveforms monitored at $n = 5, 45, 85, 125$, and 165 are shown for (a) the nonlinear and (b) linear TWFETs. The same pulses were input to the nonlinear and linear TWFETs. Black and red waveforms correspond to the gate and drain lines, respectively.

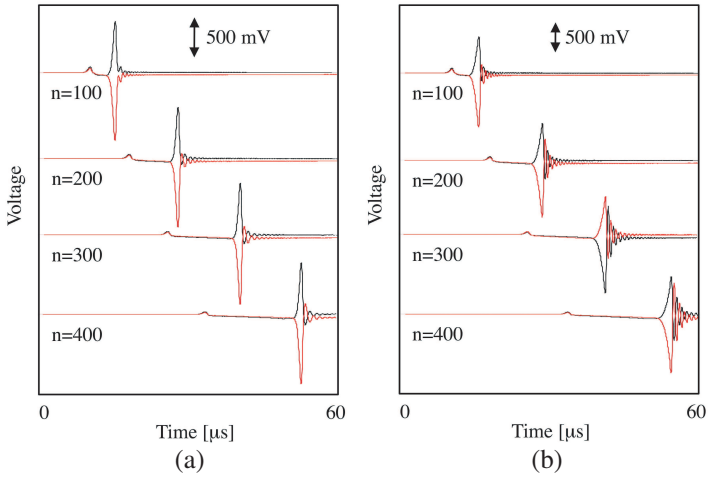

Figure 10. Pulse amplification in linear TWFETs. The total cell number was set to 500. Four temporal waveforms monitored at $n = 100, 200, 300$, and 400 are shown for (a) the nonlinear and (b) linear TWFETs. Black and red waveforms correspond to the gate and drain lines, respectively.

in Figure 10(b), although its amplitude is preserved by the FET gain. Without Schottky varactors, the length or the cell number of a TWFET has to be limited to secure the pulse bandwidth.

5. CONCLUSION

We experimentally verified that the π-mode pulse is uniquely amplified in a TWFET irrespective of the pulse amplitude. Because the c-mode pulse is significantly attenuated, pulses in a TWFET are free from modal distortions. By introducing Schottky varactors in the drain line, the resulting nonlinearity contributes to the preservation of both the amplitude and bandwidth of pulses traveling in TWFETs.

REFERENCES

1. Hirota, R. and K. Suzuki, "Studies on lattice solitons by using electrical networks," *J. of the Phys. Soc. Jpn.*, Vol. 28, 1366–1367, 1970.
2. Rodwell, M. J. W., S. T. Allen, R. Y. Yu, M. G. Case, U. Bhattacharya, M. Reddy, E. Carman, M. Kamegawa,

Y. Konishi, J. Pusl, and R. Pullela, "Active and nonlinear wave propagation devices in ultrafast electronics and optoelectronics," *Proc. of the IEEE*, Vol. 82, 1037–1059, 1994.

3. Jäger, D., "Characteristics of traveling-waves along nonlinear transmission lines for monolithic integrated circuits: A review," *Int. J. of Electron.*, Vol. 58, 649–669, 1985.
4. Wedding, B. and D. Jäger, "Phase-matched second harmonic generation and parametric mixing on nonlinear transmission lines," *Electron. Lett.*, Vol. 17, 76–77, 1981.
5. Kintis, M., X. Lan, and F. Fong, "An MMIC pulse generator using dual nonlinear transmission lines," *IEEE Microwave Wireless Compo. Lett.*, Vol. 17, 454–456, 2007.
6. Yildirim, O. O., D. S. Ricketts, and D. Ham, "Reflection soliton oscillator," *IEEE Trans. on Microwave Theory Tech.*, Vol. 57, 2344–2353, 2009.
7. Ndzana, F., A. Mohamadou, and T. C. Kofane, "Dynamics of modulated waves in electrical lines with dissipative elements," *Phys. Rev. E*, Vol. 79, 047201–047204, 2009.
8. Narahara, K., "Coupled nonlinear transmission lines for doubling repetition rate of incident pulse streams," *Progress In Electromagnetics Research Letters*, Vol. 16, 69–78, 2010.
9. Narahara, K., "Interaction of nonlinear pulses developed in coupled transmission lines regularly spaced Schottky varactors," *Progress In Electromagnetics Research Letters*, Vol. 17, 85–93, 2010.
10. McIver, G. W., "A traveling-wave transistor," *Proc. of the IEEE*, Vol. 53, 1747–1748, 1965.
11. Narahara, K. and S. Nakagawa, "Nonlinear traveling-wave field-effect transistors for amplification of short electrical pulses," *IEICE Electron. Express*, Vol. 7, 1188–1194, 2010.
12. Heinrich, W. and H. L. Hartnagel, "Wave propagation on MESFET electrodes and its influence on transistor gain," *IEEE Trans. on Microwave Theory Tech.*, Vol. 35, 1–8, 1987.
13. Narahara, K. and T. Otsuji, "Characterization of wave propagation on traveling-wave field effect transistors," *Jpn. J. of Appl. Phys.*, Vol. 37, 6328–6339, 1998.
14. Gupta, K. C., R. Garg, and I. J. Bahl, *Microstrip Lines and Slotlines*, Artech, 1979.